Intersection-Based Potential Plane Failure Detection on 3D Meshes for Rock Slopes

R. Tsui*, C. Cheung, J. Hart, W. Hou, A. Ng

GeoRisk Solutions Limited, Hong Kong

*Corresponding author
doi: https://doi.org/10.21467/proceedings.126.27

Abstract

Plane failure, a major class of rock block failures, will be considered kinematically feasible on a rock discontinuity if it fulfills certain criteria when plotted and analysed on a stereonet. However, it is often the case that this approach does not consider if a block is present above the discontinuity. With significant advances in digital surveying techniques in recent years, high-resolution 3D meshes can be readily produced for rock slope stability assessments. A semi-automatic, intersection-based approach has been developed by the authors to detect potentially adverse planar discontinuities and their intersections with planar blocks on 3D meshes. The approach involves the detection of the necessary geometrical conditions for a rock block located above a planar discontinuity and in a potentially detachable condition. The approach is considered robust in that it does not require an assumption of slope face orientation, and is not limited to checking joints within major joint sets only. A region-growing joint extraction algorithm has also been developed and used in this study. The approach is demonstrated successfully for two case studies: (I) an old road cut in Colorado, USA; and, (II) a newly formed cut slope in Hong Kong. The approach can quickly alert engineering geologists of potentially unstable blocks at risk of plane failure, especially at an early project stage when access to the rock slope may be limited.

Keywords: Rock slope, Plane failure, 3D meshes

1 Introduction

One of the goals of rock slope mapping is to identify potentially unstable blocks, which are formed along rock joints (or other types of discontinuities). Conventionally, engineering geologists measure the dipping angles and orientations of joints on the slope manually, and plot the data on stereonets to assess the kinematic feasibility of structurally controlled rock block failures. Plane failure, a major class of rock block failures, will be considered kinematically feasible on a joint if it fulfills certain criteria when plotted and analysed on stereonets (Wyllie and Mah, 2004). However, as these criteria assume rock slope uniformity and do not consider intersection relationships between individual joints, it is often the case that some of the detected adverse joints are not actually associated with potentially unstable blocks. The analysis also has limitations for rock slopes with complex geometries. In addition, whilst on site observations and measurements are critical, measurements taken directly on the slope can be time-consuming and subjective, with data accuracy and relevance dependent on the skill and experience of the practitioners involved.

With significant recent advances in digital surveying techniques such as photogrammetry and laser scanning, high-resolution 3D meshes can be readily produced for rock slopes, and can be used to provide innovative solutions to these challenges. Numerous new software, algorithms and workflows

Proceedings DOI: 10.21467/proceedings.126; Series: AIJR Proceedings; ISSN: 2582-3922; ISBN: 978-81-954993-7-3

have been developed or proposed in recent years for digital rock slope mapping (e.g. Assali et al., 2014; Riquelme et al. 2014, 2016; Buyer, 2020). While workflows for the kinematic analysis of data generated from 3D point clouds have been proposed (e.g., Matasci et al., 2018; Menegoni et al., 2019), these are based on traditional kinematic analysis approaches, or are limited to considering joints within major joint sets.

To overcome these issues, the authors propose an alternative and innovative, semi-automatic approach to detect potential plane failures using high-resolution 3D meshes, based on intersections between the planar joints and the associated blocks above. The approach does not require slope orientation assumptions or major joint set identification and assessment prior to the analysis.

1.1 Terminology

For readers less familiar with 3D data, terminology related to 3D data such as “point cloud”, “mesh” and “faces” are provided in Figure 1. The term “normal” refers to a unit vector perpendicular to a planar entity, such as a joint plane or a mesh face (i.e., “poles” to planes plotted on stereonets). A point or a vertex can also have a normal which is perpendicular to its locally best-fit plane.

Figure 2 illustrates terms related to joint orientation. For convenience, the dip angle δ and the strike $\boldsymbol{S}$ of a joint used in our study are used slightly differently from conventions (for overhanging cases), and are related to the joint normal $\boldsymbol{n_j}$ as follows:

$$\delta = \cos^{-1}(\boldsymbol{n_j} \cdot \boldsymbol{z}) \text{ (note: } \delta < 90º \text{ for overhanging cases here)} \quad (1)$$

$$\boldsymbol{S} = \frac{\boldsymbol{z} \times \boldsymbol{n_j}}{|\boldsymbol{z} \times \boldsymbol{n_j}|} \text{ (note: } \boldsymbol{S} \text{ is towards dip direction + 90º for overhanging cases here)} \quad (2)$$

where **z** is the unit vector along z-axis (upwards)

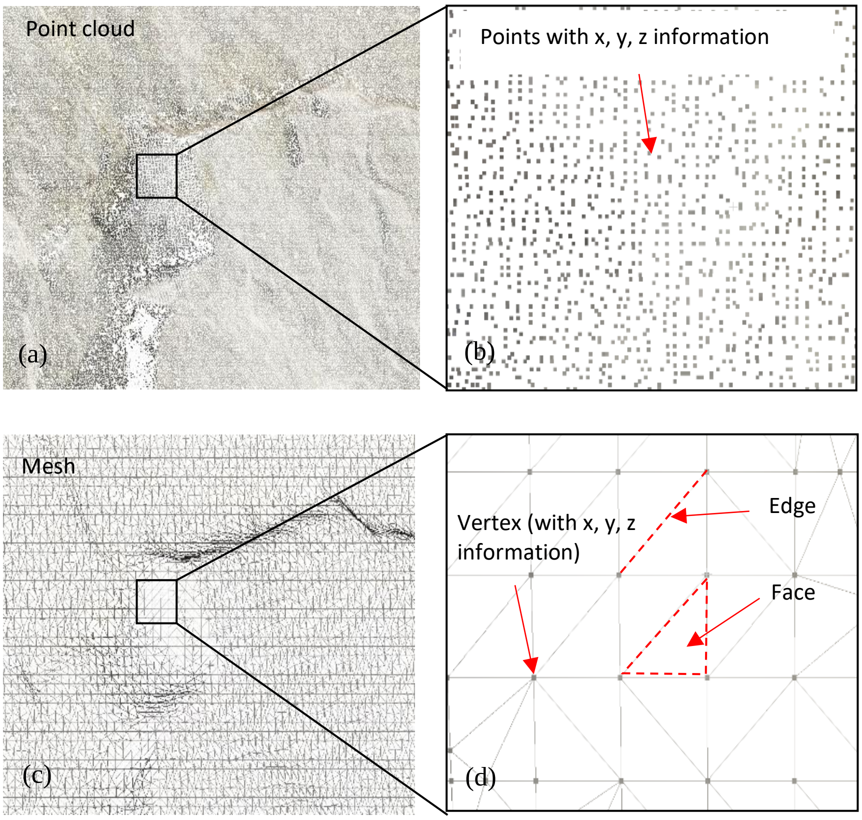

Figure 1: Terminology for 3D data

Proceedings DOI: 10.21467/proceedings.126
ISBN: 978-81-954993-7-3

Series: AIJR Proceedings
ISSN: 2582-3922

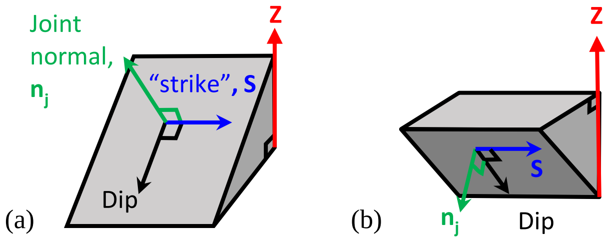

Figure 2: Terminology for joint orientation (slightly different from convention for overhanging case)

1.2 Proposed Approach for the Detection of Potentially Adverse Planar Joints

If a block can slide along a planar joint, its lowest, frontal face should be unobstructed. This means that the block's frontal face should intersect with the planar joint and form a concave rock edge. The joint in this case is daylighting. These intersections are referred to as "daylight-indicating intersections" for this approach.

As illustrated in Figure 3, suppose all intersections made by the daylighting planar joint (effectively these form its outline, if no isolated blocks are present on top) are arranged in a clockwise orientation, then we can measure the angle between the joint's strike $\boldsymbol{S}$ and an intersection as α. For an intersection between the planar joint and the front of the block, which cuts above the joint (Figure 3b), the α would be small. In contrast, if the joint only intersects with the lateral side of a block (Figure 3c), the α would be 90º. For cases in between, some sharp blocks may have a minimum α of 30º (Figure 3d). However, it would be rare that a detachable block does not have a side with α < 80º (Figure 3e). In this study, 60º is used as a cut-off value for α. In addition, if the intersection "cuts below" the joint (i.e. intersection with the rear of a block), α = 90º to 180º (Figure 3f).

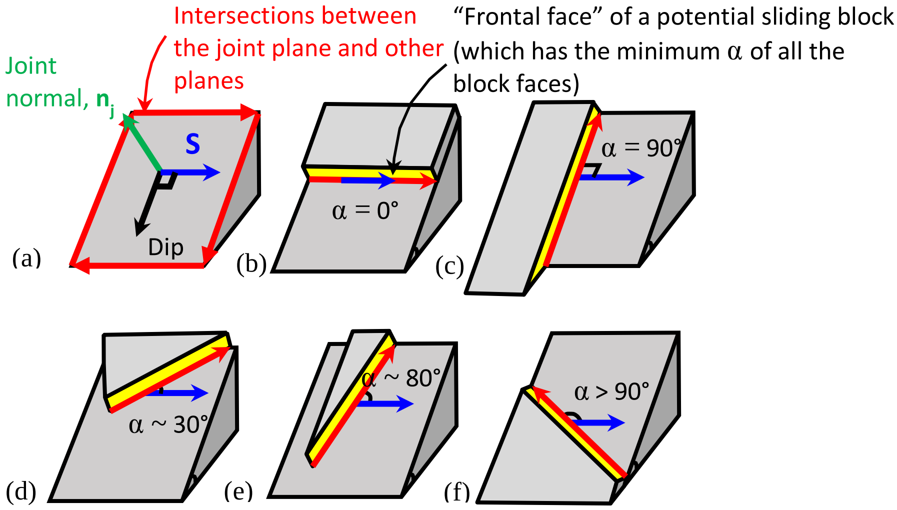

Figure 3: α in different configurations of a planar block and a planar joint

A daylight-indicating intersection therefore satisfies two conditions:

(i) it has $\alpha < \alpha_{tol}$ (angle of tolerance for α, set to 60 º in this study), and

(ii) it is concave.

Considering natural undulations on the rock may create noises, it would be desirable to set a minimum length, L_{min}, for a daylight-indicating intersection to be flagged. In addition, the associated planar joint should be steeper than the friction angle along the joint surface to be regarded as adverse. However, as indicated earlier, this approach does not need to assume an overall orientation for the slope face.

2 Methodology

The proposed method comprises four main stages: (1) joint extraction; (2) estimation of joint orientations; (3) detection of daylight-indicating intersections; and, (4) consideration of minimum block width.

Prior to meshing, the point cloud of the rock slope is cleaned such that points not belonging to the rock mass (e.g. vegetation, man-made features, soil deposits, etc.) are removed. Meshing was carried out in CloudCompare (2017), using the Poisson Surface Reconstruction plugin. Section 2.7 provides a list of python packages used in our implementation.

2.1 Joint Extraction

Since the outline of the exposed surface of the joint will be used to represent intersections made by the joint, the outline should be extracted accurately. In addition, random joints should also be evaluated. Whilst a number of plane segmentation schemes have been developed for digital rock joint mapping, which have worked well for their intended purposes, there are a number of limitations when applying these schemes to our approach. For example, some only extract those joints within major joint sets (e.g. Riquelme et al. 2014), and some do not preserve the outline of the joints accurately (e.g. Dewez et al. 2016). Therefore, for the purpose of this study, we have adopted a region-growing approach similar to those described by Vöge et al. (2013) and Wang et al. (2017).

2.1.1 Edge Removal

The first step for joint extraction is to remove edges of the rock mass, such that flat planes with different orientations can be segmented as isolated small meshes (i.e. “seed planes”).

Mesh faces at rock edges can be identified by high surface curvature. To estimate the local curvature (σ) of a face, eigendecomposition is carried out on the covariance matrix of the centroids of its neighboring faces. This yields three pairs of orthogonal eigenvectors and eigenvalues (λ_1, λ_2 and λ_3, where $\lambda_1 \geq \lambda_2 \geq \lambda_3$). Curvature σ can be estimated by Pauli et al. (2002):

$$\sigma = \frac{\lambda_3}{\lambda_1 + \lambda_2 + \lambda_3} \tag{3}$$

The variation of σ on a simple object is illustrated on Figure 4a. In this study aggressive thresholds are used (e.g. removing 40-80% of the total mesh faces) to ensure that planes with different orientations can be completely separated. This step turns the original mesh into a “patchy” mesh, which is in fact a group of disconnected small meshes.

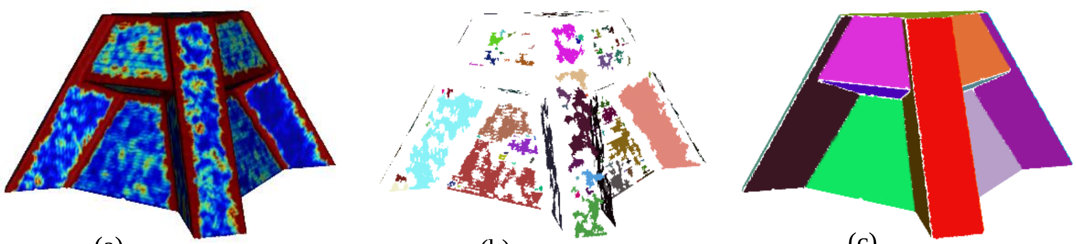
(a) (b) (c)

Figure 4: Region-growing joint extraction algorithm on a simple object

2.1.2 Seed Planes

By analyzing mesh connectivity, each isolated small mesh in the "patchy" mesh is then labelled as a seed plane (Figure 4b). Initial plane-fitting by principal component analysis (i.e. PCA, further discussed in Section 2.2) is carried out on each seed plane (with face centroids) to derive its plane normal, $\boldsymbol{n_s}$. The normals of all of the mesh faces on the seed plane are then uniformly re-orientated in the direction same as $\boldsymbol{n_s}$. This is to ensure that in the later region-growing stage, mesh faces on the same seed plane can stay together.

2.1.3 Region-growing

In the previous two steps, a joint may be separated into two or more seed planes due to undulations. In addition, mesh faces close to the rock edges or corners are not preserved well during the aggressive edge removal process. The region-growing stage aims to grow the seed planes back to their full extents.

For each seed plane M_s, which has normal $\boldsymbol{n_s}$, the angular difference ϑ_f between itself and a mesh face f in the original mesh M with face normal $\boldsymbol{n_f}$ is:

$$\vartheta_f = \cos^{-1} (\boldsymbol{n_s} \cdot \boldsymbol{n_f}) \tag{4}$$

If θ_f is small enough, f can be regarded as co-planar with M_s. In our study, the angle of tolerance, ϑ_{tol}, is set at 15º-30 º based on rock mass characteristics. If $\vartheta_f < \vartheta_{tol}$, then f is added to a temporary mesh, M'. This is evaluated for every mesh face f in the original mesh M. All components connected to M_s in M', including previously unclassified mesh faces and other seed planes, will be combined into M_s. The normals of these newly added components will now also re-orient with $\boldsymbol{n_s}$. This process is then iterated over all of the remaining seed planes. At the end of the stage, each grown seed plane is regarded as a joint plane (Figure 4c).

2.2 Estimation of Joint Orientation

After extracting the joints, the joint orientations are estimated by PCA, which can minimize the orthogonal distances between the input data and the fitted plane.

Each extracted joint is now represented by its mesh, M_j. For each joint, PCA is carried out by eigen composition on the covariance matrix of the mesh vertices on M_j, which gives three pairs of orthogonal eigenvectors ($\boldsymbol{e_1}$, $\boldsymbol{e_2}$, $\boldsymbol{e_3}$) and eigenvalues (λ_1, λ_2 and λ_3, where $\lambda_1 \geq \lambda_2 \geq \lambda_3$). The eigenvector $\boldsymbol{e_3}$, associated with the smallest eigenvalue λ_3, represents the direction that accounts for the least variance in the scatter of the vertices on M_j. This is effectively the normal to the best-fit plane of M_j. In other words, joint normal $\boldsymbol{n_j} = \boldsymbol{e_3}$ (or $-\boldsymbol{e_3}$ if $\boldsymbol{e_3}$ is opposite to most of the face normals on M_j).

The dip angle δ and strike $\boldsymbol{S}$ for each extracted joint can then be obtained from equations (1) and (2).

2.3 Detection of Daylight-Indicating Intersections

As mentioned in Section 1.2, a daylight-indicating intersection has (i) $\alpha < \alpha_{tol}$ and is (ii) concave. In the implementation, conditions (i) and (ii) are checked for each mesh edge on the outline of M_j. Since the outline of M_j may be ragged, spline smoothing is applied. In addition, edges which are also part of the outline of the original mesh M are excluded as they do not represent real intersections between planes (Figure 5b).

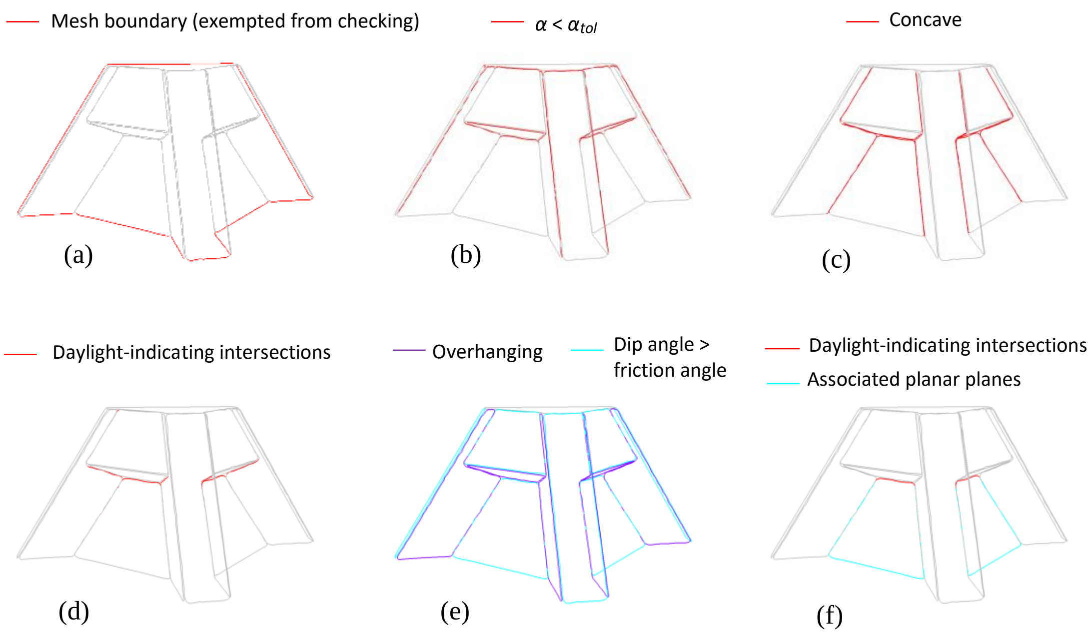

Figure 5: Plane failure detection on a simple object (same object as in Figure 4)

2.3.1 Identification of Intersections "Above" The Joint

As illustrated in Figure 3(a), the mesh edges on the outline of M_j are first arranged in a clockwise direction around the joint normal $\boldsymbol{n}_j$. The vertices on the outline are [$\boldsymbol{v}_1$, $\boldsymbol{v}_2$, ..., $\boldsymbol{v}_n$]. An edge between two vertices $\boldsymbol{v}_i$ and $\boldsymbol{v}_{i+1}$ is represented by $\boldsymbol{E}_i = \boldsymbol{v}_{i+1} - \boldsymbol{v}_i$. If the displacement from an edge $\boldsymbol{E}_i$ to the center of the mesh is $\boldsymbol{l}_i$, the cross product $\boldsymbol{l}_i \times \boldsymbol{E}_i$ for most edges should roughly align with $\boldsymbol{n}_j$ if the edges are in a clockwise direction. If not, then the outline vertices need to be sorted in the opposite direction. After the ordering is fixed, the angle α_i between each edge $\boldsymbol{E}_i$ and the strike of the joint $\boldsymbol{S}_j$, can be calculated by:

$$\alpha_i = \cos^{-1}\left(\frac{\boldsymbol{E}_i}{|\boldsymbol{E}_i|} \cdot \boldsymbol{S}_j\right) \tag{5}$$

Based on discussion in Section 1.2, an angle of tolerance α_{tol} is set at around 60º. If $\alpha_i < \alpha_{tol}$, the edge will be regarded as "cutting above" the joint. Figure 6 demonstrates the effect of α < 60º on an object with circular holes.

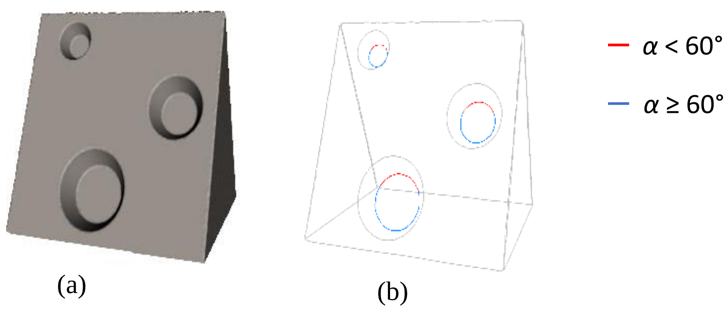

Figure 6: (a) A simple object with circular holes (b) α around the circular holes

2.3.2 Estimation of Signed Local Curvature (Concavity)

Whether a mesh edge $\boldsymbol{E_i}$ is concave or not can be estimated by the curvature of either one of its vertices, $\boldsymbol{v_i}$. In this study, the "concavity" (c_i) of $\boldsymbol{v_i}$ is estimated by the mean positional differences between $\boldsymbol{v_i}$ and its k-nearest neighbors along $\boldsymbol{n_v}$, i.e., the normal of $\boldsymbol{v_i}$ (Figure 7, equation (6)). c_i is positive for $\boldsymbol{v_i}$ at concave rock corner or edges, and is negative for convex cases. To reduce sensitivity, a threshold is set to ignore slightly positive c. Concave edges for a simple object is identified in Figure 5(c).

$$c_i = (\overline{\boldsymbol{v_k}} - \boldsymbol{v_i}) \cdot \boldsymbol{n_v} \tag{6}$$

where $\overline{\boldsymbol{v_k}}$ is the mean position of the nearest neighbors of $\boldsymbol{v_i}$.

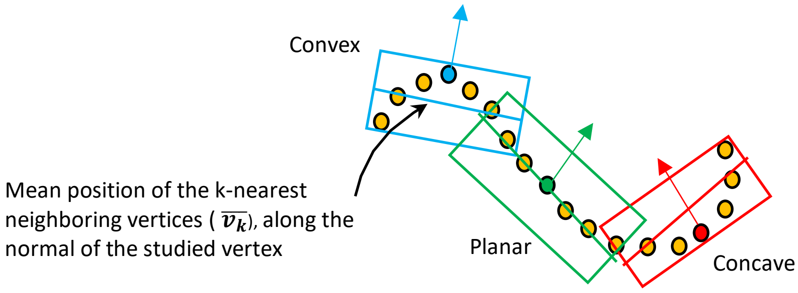

Figure 7: Estimation of signed local curvature

2.4 Minimum Width of Potential Planar Block

As mentioned in Section 1.2, daylight-indicating intersections are required to be longer than L_{min}, to be flagged. In our approach we evaluate the projected length along the joint's strike ($\boldsymbol{S_j}$) against L_{min}. In other words, a connected segment of N mesh edges [$\boldsymbol{E_1}$, $\boldsymbol{E_2}$, ..., $\boldsymbol{E_N}$] which satisfy conditions (i) and (ii) needs to further satisfy equation (7) below. On the other hand, mesh edges on daylight-indicating intersections might locally fail to satisfy conditions (i) and (ii). These are ignored if less than a certain length (0.1m used in the case studies).

$$\sum_{i=1}^{N} \boldsymbol{E_i} \cdot \boldsymbol{S_j} > L_{min} \tag{7}$$

2.5 Special Case

In rare cases, there may be an isolated "island block" on top of a planar joint. In such case, the intersections between the block and the joint will not be represented as part of the outline of the mesh M_j, but as a hole within M_j. The approach described above can still be applied to find daylight-indicating intersections in such holes, although in the procedures described in Sections 2.3.1, the edges should be orientated anticlockwise instead of clockwise. Case study II (Section 4.2) takes this special case into account. However, in most cases these holes are merely slightly elevated undulations instead of isolated blocks.

2.6 Presentation

If a joint contains any segments satisfying equation (7), and that the joint is steeper than the friction angle, it is flagged as a potentially adverse planar joint, or an overhanging joint if $\delta > 90º$. The polylines of the daylight-indicating intersections and the associated joint outlines are output as dxf files, which can be viewed in CAD and GIS.

2.7 Implementation in Python

Our approach is implemented in Python scripts. The overall analysis relies heavily on a number of widely used, well tested Python packages, as shown in Table 1.

Table 1. Python packages used in analysis

Python packages	Usage
Trimesh (Dawson-Haggerty et al. 2019)	Mesh input / output, general mesh manipulations
NumPy (Harris et al. 2020)	Eigendecomposition for PCA, and other operations on matrices
SciPy (Virtanen et al. 2020)	Finding connected components on meshes; spline smoothing for joint outline; k-nearest neighbor search
NetworkX (Hagberg et al. 2008)	Finding mesh outline and holes
ezdxf (2021)	Writing dxf files

3 Applications

The approach described above is applied to two case studies to detect potentially adverse planar joints. The results are then compared to that obtained from traditional rock slope mapping and kinematic analysis. Case study I is a roadside cut slope in Ouray, Colorado, USA (Lato et al., 2013) (Figure 8a). Case study II is a newly-formed cut slope in Hong Kong (Figure 8b). Information of the datasets and key parameters used in the analyses are summarized in Tables 2 and 3.

(a) (b)

Figure 8: (a) Case study I – an existing roadside cut slope in Ouray, Colorado, USA; (b) Case study II – a newly formed cut slope in Hong Kong

Table 2. Information of the analyzed datasets

	Case Study I	Case Study II
Lithology	Quartzite	Granite
Approximate slope dimensions	20m long × 15m high	16m long × 8m high (max.) (W-facing), 10 long × 3m high (N-facing)
Approximate slope orientation(s)	295º/75º	258º/80º, 348º/80
Method of data acquisition	Terrestrial laser scanning	Structure-from-Motion photogrammetry (from UAV photos)
Point spacing	< 20mm	< 5mm
Total No. of faces on analyzed mesh	2,533,930	1,105,468

Proceedings DOI: 10.21467/proceedings.126
ISBN: 978-81-954993-7-3

Series: AIJR Proceedings
ISSN: 2582-3922

Table 3. Key parameters used in potential planar sliding joint detection analyses

	% of mesh face removed based on σ	**ϑ_{tol} (º)**	**α_{tol} (º)**	**% of positive *c* values ignored**	**Friction angle (º)**	**L_{min} (m)**
Case Study I	45	20	60	50	35	0.2
Case Study II	80	17	60	50	40	0.2

3.1 Case I: Roadside cut slope in Ouray, Colorado, USA

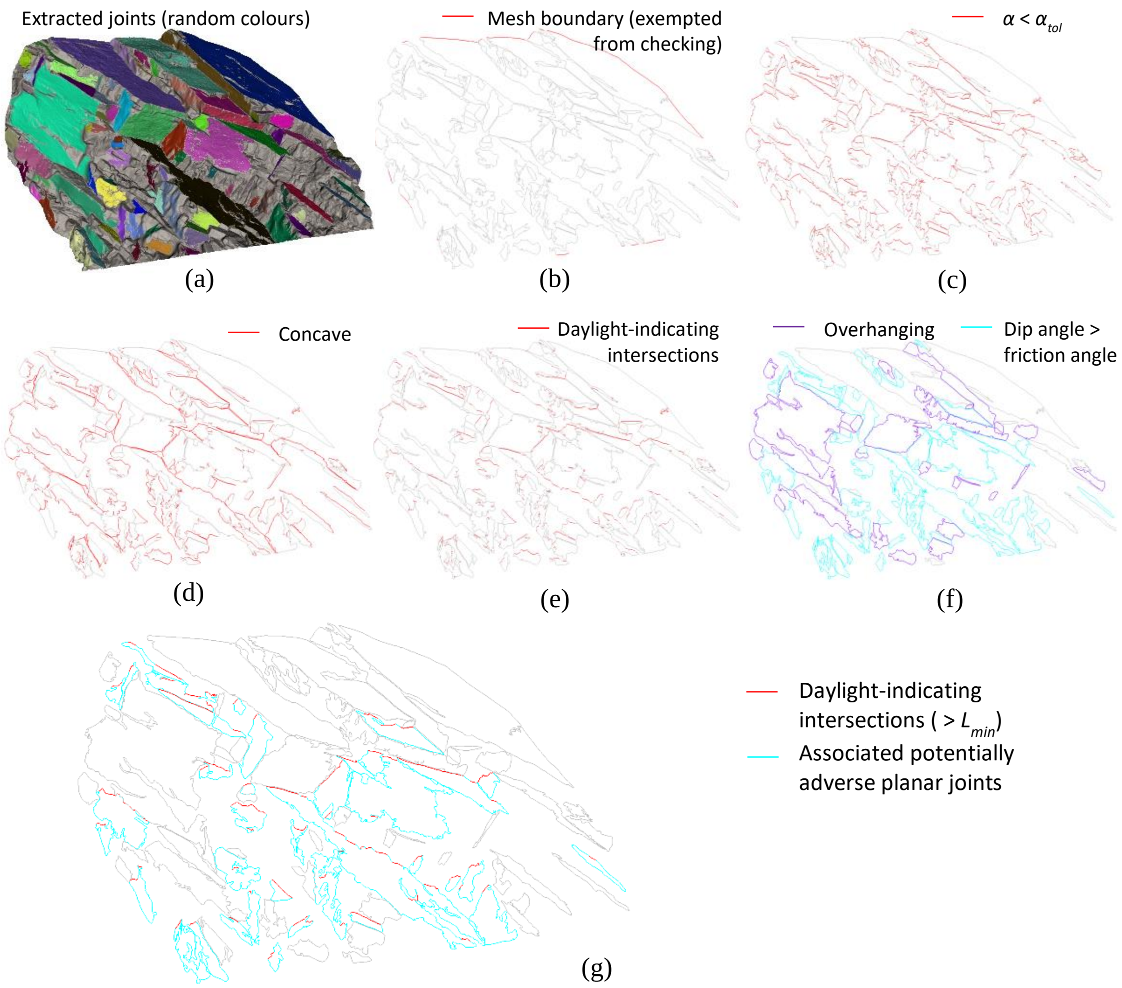

Figure 9: Results of plane failure detection for Case Study I

The dataset was originally hosted on the Rockbench open repository (Lato et al. 2012) and has been used in several digital rock joint mapping research (e.g., Riquelme et al. 2014; Chen et al. 2016; Zhang et al. 2020). The rock slope contains a set of persistent planar joints dipping at approximately 35º, obliquely towards the road. For testing purposes, the friction angle is set to 35º so that more joints within the set are included as potentially adverse.

In the joint extraction stage, a total of 90 joints were extracted. The results are reasonable based on visual inspection of the mesh. Applying our approach, 39 potentially adverse planar joints were identified, which contain a total of 68 daylight-indicating intersections. The intermediate and final outputs are displayed in Figures 9a-f and 9g respectively.

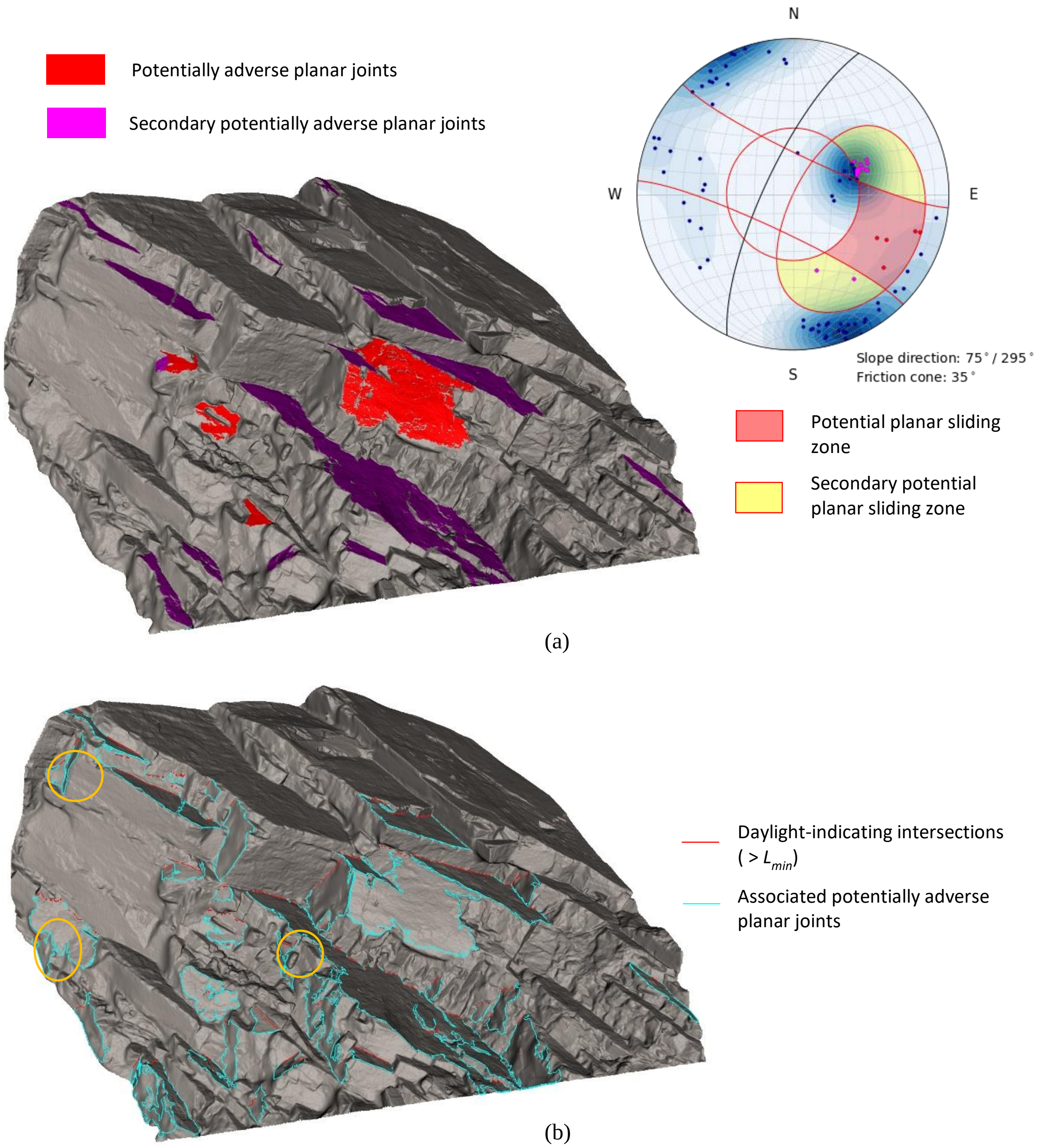

Figure 10: (a) Case Study I results traditional kinematic analysis; (b) our results for comparison

Using the same extracted joint data, the traditional kinematic analysis identified 5 joints within the main planar sliding zone (± 20° lateral limits), and 15 joints within the secondary planar sliding zones (Figure 10a). Out of a total of 20 joints, 18 are also identified by our approach. The other 2 joints are not associated with blocks above. The majority of these 18 joints appear valid to be flagged (i.e. highlighted) as potentially adverse.

Among the joints which are only detected by our approach, some appear valid to be flagged but is missed by the traditional approach, although the potential blocks are rather small (three circled in Figure 10b). However, some are indeed irrelevant cases where the detected daylight-indicating intersections are merely undulations. In addition, a significant portion of the irrelevant cases are in fact associated with wedge-sliding mechanism.

The case study demonstrates that without considering the slope orientation, our approach can potentially yield more relevant results than the traditional kinematic analysis. In addition, some potential wedge joints are also flagged as potentially adverse.

3.2 Case II: A Newly-Formed Cut Slope in Hong Kong

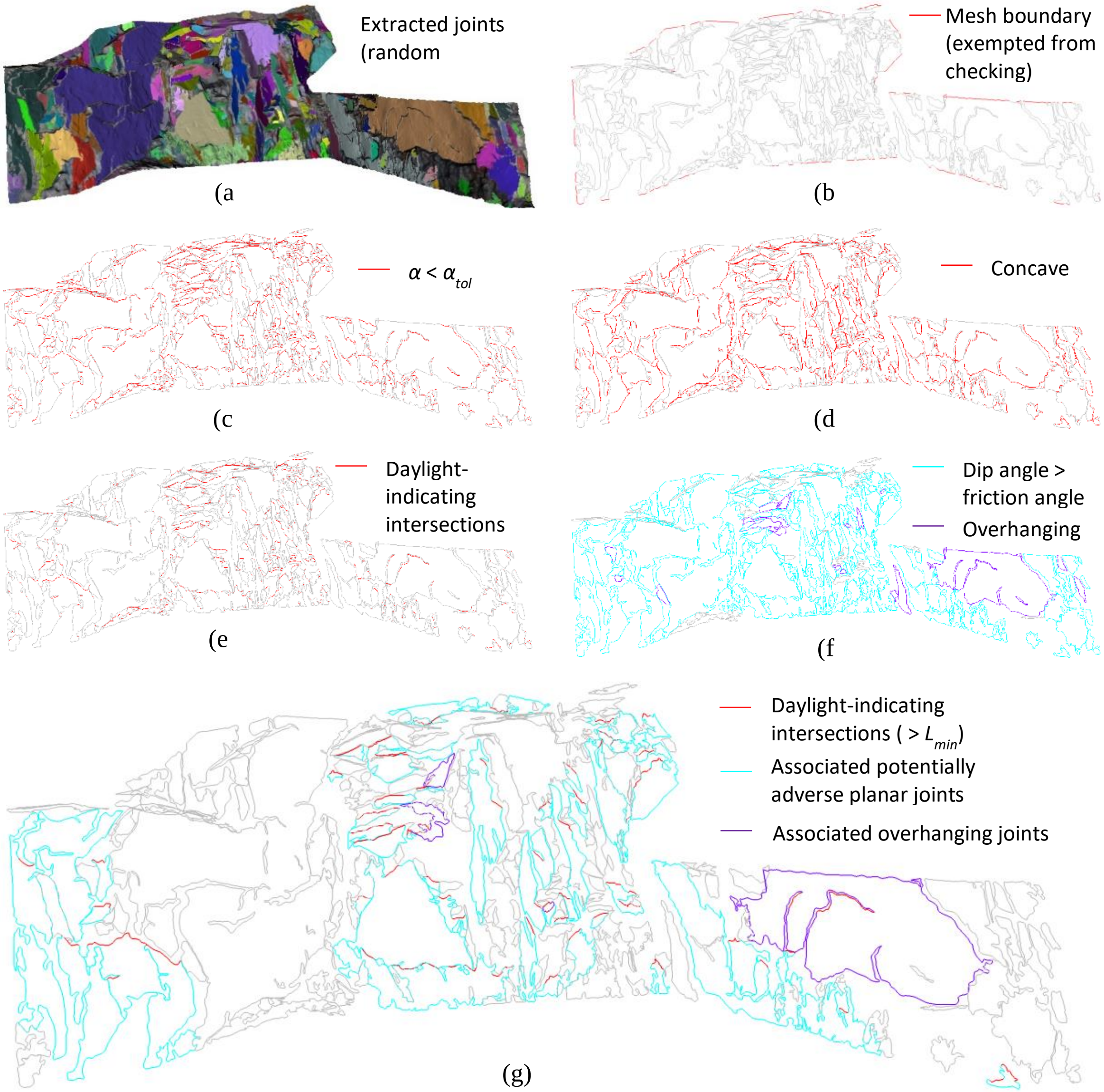

Figure 11: Results of plane failure detection for Case Study II

The cut slope was newly excavated at the time of the survey, which was completed prior to slope treatments. The cut slope contains a north-facing portion and a west-facing portion. This slope was selected for analysis for three reasons: (1) the lower part (< 4m high) has been mapped by the authors on site; and, (2) potentially unstable rock blocks were identified during this survey; and, (3) the geometry of the rock slope is not uniform, requiring multiple kinematic analyses using traditional methods.

In the joint extraction stage, a total of 279 joints were extracted. Applying our approach, 56 potentially adverse planar joints were identified, which contain a total of 75 daylight-indicating intersections. The intermediate and final outputs are displayed in Figures 11a-f and Figure 11g respectively.

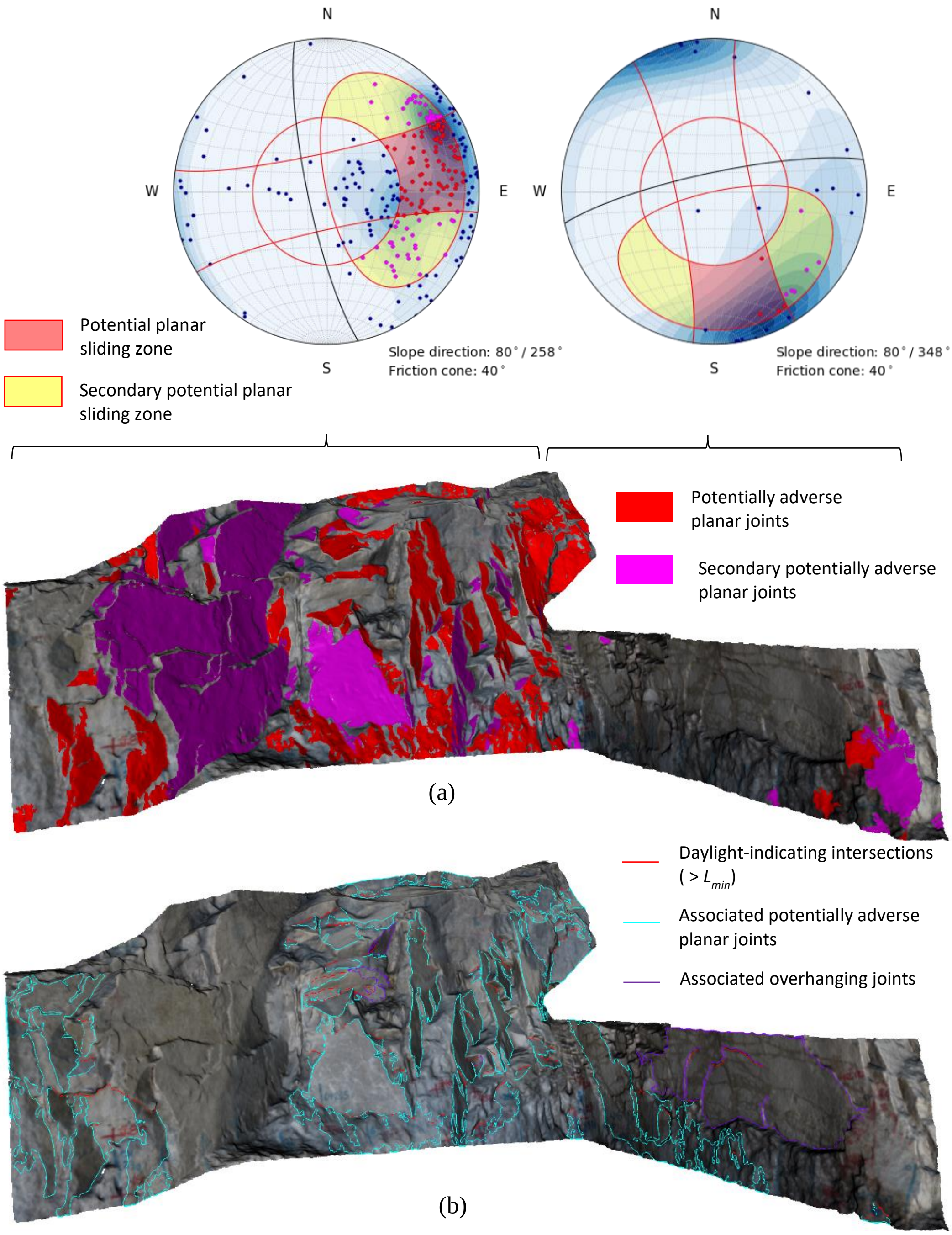

Figure 12: (a) Case Study II results - traditional kinematic analysis; (b) our results for comparison

As the slope contains two portions with two different orientations, it is required to be segmented into two parts for traditional kinematic analysis (Figure 12a). Using the same extracted joint data, the traditional kinematic analysis approach identifies a total of 83 joints within the main planar sliding zone, and 60 joints within the secondary planar sliding zones (Figure 12a). Out of a total of 143 joints, 38 are identified by our own approach.

Proceedings DOI: 10.21467/proceedings.126
ISBN: 978-81-954993-7-3
Series: AIJR Proceedings
ISSN: 2582-3922

Within <4m height of the analyzed slope area, our on-site mapping identified one potentially unstable planar block, two potentially unstable wedge blocks, and a small area of potentially raveling blocks. In both approaches, the potentially adverse planar joint and one of the potentially adverse wedge joints are detected (circled in black in Figure 12b). The other wedge sliding case is not detected since the associated joints have limited exposed area (i.e. traces) and are not extracted. For the raveling case, the blocks are not sitting on planar joints.

From the mapping results, it would appear that both methods produce a large number of false positives. However, some of the false positives are in fact valid to be flagged or highlighted, meaning it would indeed require further checking to see if the block on the flagged joint is detachable. A significant portion of false positives identified in our approach belong to this case. Some of these cases are not detected by traditional kinematic analysis (circled in orange in Figure 12b). As for cases which are indeed irrelevant, the detected daylight-indicating intersections are mostly stepped undulations on closely spaced, persistent joints. In comparison, the traditional kinematic analysis approach produces more irrelevant cases (i.e., false alarms), which is expected given a large number of exposed joints are subvertical joints parallel to the slope face. It is also worth mentioning that slope angle and orientation estimation is somewhat subjective. If it was estimated at 70°, the potentially adverse planar joint identified on site (δ = 74°) would be too steep to be in the daylight envelope and will be missed.

4 Discussion

4.1 Advantages of the Approach

The case studies demonstrate that both the intersection-based approach and the traditional kinematic analysis are useful in highlighting joints susceptible to plane failure on 3D meshes.

Advantages of our approach over traditional kinematic analysis for plane failure are:

- The approach involves more flexibility as there is no need to estimate a slope orientation, which may be difficult for some slopes with complex geometry.
- It is not necessary to sub-divide the slope for every change in slope direction.
- It allows direct visualization of the potentially adverse planar joints alongside their intersection with the planar blocks, which is convenient for checking purposes.
- The widths of the potentially unstable planar blocks can be estimated at a glance.
- Fewer missed cases.
- Fewer false alarms, when a subvertical joint set parallel to the slope face is present.

4.2 Limitations

There are a number of intrinsic limitations with the intersection-based approach. Firstly, joint traces (i.e. joints with limited exposed area, appearing as lines on the rock slope) are not considered. Secondly, similar to traditional kinematic analysis, the assumption that all joints have the same assumed friction angle is an over-simplification, given that joint-infilling can be present at some joints, which is not checked by our approach and requires field verification. Thirdly, our approach does not check the height of the potential sliding block, causing it to be sensitive to stepped undulations on joint planes. Fourthly, assuming all joints are accurately extracted and all have the same assumed friction angle, the conditions used in detection for detachable blocks on planar joints are in logic terms "necessary but not sufficient". This is because detachable blocks would also have side and back release mechanisms, which are not checked in our approach, meaning that there may be significant false positives with our approach.

4.3 Parameters and Computation Time

Although systematic sensitivity analysis is not available, the case studies show that using the same preset values for α_{tol}, c and L_{min} in our approach, yields reasonable results, requiring no mesh-specific parameter tuning. L_{min} is adjustable based on the project purpose. In comparison, our joint extraction algorithm is not as reliable and is rather sensitive to the σ and ϑ_{tol} parameters. Optimal values for these two parameters are mesh-specific and require trial-and-error tuning. The joint extraction algorithm proposed in this study can probably be replaced by other mesh-based plane segmentation algorithms of choice, as long as the outline of the extracted joints are reasonably accurate, and, ideally, random joints are extracted.

The total computation time is reasonably short since we leverage a number of high-performance Python packages (e.g., NumPy and SciPy). On a computer with Intel Core i7-9750H and 16 GB RAM, the total computation times (i.e. from loading pre-segmented mesh to exporting .dxf files) for both cases were < 3 minutes. Joint extraction took approximately 90% of total computation time. On segmented meshes, plane failure detection took under 20s for the two case studies. Further testing can be carried out to see how this scales to larger projects. Further optimization, such as rewriting some of the Python loops in C++, are also possible.

4.4 Potential Useful Applications and Further Investigations

Potential useful applications for this technique are:

- Slopes without sufficient access can be surveyed by remote sensing techniques first. Potentially adverse planer joints can be flagged before safe access becomes available for closer inspections and measurements.
- This method can supplement the results of direct mapping so that potentially adverse planar joints are not overlooked. This is especially useful when the rock mass is heavily fractured, and the chance of overlooking critical joints is increased.

Potential further investigations are:

- Estimation of the planar block's height for screening out the stepped undulations
- Extension to other rock slope failure modes, such as wedge and toppling failure

5 Conclusions

This study proposes and describes an alternative, semi-automatic, intersection-based approach to detect potentially adverse planar joints and their daylighting intersections on 3D meshes of rock slopes. A region-growing joint extraction approach is also proposed and used in this study. The proposed plane failure the detection of the necessary geometrical conditions for a rock block located above a planar discontinuity and in a potentially detachable condition. Our approach is demonstrated successfully for two case studies involving real rock slopes, one of which is a mapped rock slope in Hong Kong. Benchmarking against traditional kinematic analysis for planar sliding, our approach yields more relevant results and is more flexible and better suited for engineering needs. While these semi-automatic techniques cannot replace field verification by geologists, our approach can quickly alert engineering geologists of potentially unstable blocks at risk of plane failure, especially at an early project stage when access to the rock slope may be limited.

6 Acknowledgements

The laser scanner data from Case Study I was retrieved from Dr. Riquelme's personal website (https://personal.ua.es/en/ariquelme/a-new-approach-for-semi-automatic-rock-mass-joints-recognition-from-lidar-data.html). The dataset was formerly hosted on the Rockbench open repository (www.rockbench.org). Our approach was developed following a benchmarking exercise instigated by the GEO in 2020 and we would like to thanks the organizers.

References

[1] Assali, P., Grussenmeyer, P., Villemin, T., Pollet, N., & Viguier, F. 2014. Surveying and modeling of rock discontinuities by terrestrial laser scanning and photogrammetry: Semi-automatic approaches for linear outcrop inspection. *Journal of Structural Geology*, 66: 102-114.

[2] Buyer, A., Aichinger, S., & Schubert, W. 2020. Applying photogrammetry and semi-automated joint mapping for rock mass characterization. *Engineering Geology*, 264: 105332.

[3] Chen, J., Zhu, H., & Li, X. 2016. Automatic extraction of discontinuity orientation from rock mass surface 3D point cloud. *Computers & Geosciences*, 95: 18-31.

[4] CloudCompare (version 2.9). 2017. Retrieved from http://www.cloudcompare.org/

[5] Dewez, T.J., Girardeau-Montaut, D., Allanic, C., & Rohmer, J. 2016. Facets: A CloudCompare Plugin To Extract Geological Planes From Unstructured 3d Point Clouds. *Int. Arch. Photogramm. Remote Sens. Spatial Inf. Sci*., XLI-B5: 799-804.

[6] Dawson-Haggerty et al. 2019. Trimesh (version 3.2.0). https://trimsh.org/ezdxf (version 0.16). 2021.ezdxf.mozman.at/

[7] Hagberg, A. A., Schult, D. A., & Swart, P. J. 2008. Exploring Network Structure, Dynamics, and Function using NetworkX. In G. Varoquaux, T. Vaught, & J. Millman (ed.), *Proceedings of the 7th Python in Science Conference, Pasadena, 2008*.

[8] Harris, C. R., Millman, K. J., van der Walt, S. J., Gommers, R., Virtanen, P., Cournapeau, D., . . . Oliphant, T. E. 2020. Array programming with NumPy. *Nature*, 585: 357–362.

[9] Lato, M., Kemeny, J., Harrap, R.M., & Bevan, G. 2013. Rock bench: Establishing a common repository and standards for assessing rockmass characteristics using LiDAR and photogrammetry. *Computers & Geosciences*, 50: 106-114.

[10] Pauly, M., Gross, M., & Kobbelt, L. P. 2002. Efficient simplification of point-sampled surfaces. In *IEEE Visualization, October 2002. VIS 2002*. IEEE.

[11] Riquelme, A. J., Abellán, A., Tomás, R., & Jaboyedoff, M. 2014. A new approach for semi-automatic rock mass joints recognition from 3D point clouds. *Computers & Geosciences*, 68: 38-52.

[12] Riquelme, A. J., Tomás, R., & Abellán, A. 2016. Characterization of rock slopes through slope mass rating using 3D point clouds. *International Journal of Rock Mechanics and Mining Sciences*, 84: 165-176.

[13] Virtanen, P., Gommers, R., Oliphant, T.E., Haberland, M., Reddy, T., Cournapeau, D., . . .SciPy 1.0 Contributors. 2020. SciPy 1.0: Fundamental Algorithms for Scientific Computing in Python. *Nature Methods*, 17, 261–272.

[14] Vöge, M., Lato, M.J., & Diederichs, M.S. 2013. Automated rockmass discontinuity mapping from 3-dimensional surface data. *Engineering Geology*, 164: 155-162.

[15] Wyllie, D. C., & Mah, C. 2004. Rock slope engineering. CRC Press.

[16] Wang, X., Zou, L., Shen, X., Ren, Y., & Qin, Y. 2017. A region-growing approach for automatic outcrop fracture extraction from a three-dimensional point cloud. *Computers & Geosciences*, 99: 100-106.